

# Gravitational waves from type II axion-like curvaton model and its implication for NANOGrav result

Masahiro Kawasaki<sup>(a,b)</sup> and Hiromasa Nakatsuka<sup>(a)</sup>

<sup>(a)</sup>*ICRR, The University of Tokyo, Kashiwa, Chiba 277-8582, Japan*

<sup>(b)</sup>*Kavli IPMU (WPI), UTIAS, The University of Tokyo, Kashiwa, Chiba 277-8583, Japan*

## Abstract

The recent report of NANOGrav is gathering attention since its signal can be explained by the stochastic gravitational waves (GWs) with  $\Omega_{\text{GW}} \sim 10^{-9}$  at  $f \sim 10^{-8}$  Hz. The PBH formation scenario is one of the candidates for the NANOGrav signal, which can simultaneously explain the observed  $30M_{\odot}$  black holes in the binary merger events in LIGO-Virgo collaboration. We focus on the type-II axion-like curvaton model of the PBH formation. In type II model the complex field whose phase part is the axion rolls down from the origin of the potential. It is found that type II model achieves the broad power spectrum of the density perturbations and can simultaneously explain the LIGO-Virgo events and the NANOGrav signal. We also improve the treatment of the non-Gaussianity of perturbations in our model to estimate the amplitude of the induced GWs precisely.

# 1 Introduction

North American Nanohertz Observatory for Gravitational Waves (NANOGrav) is one of the Pulsar-timing-array experiments, which has been trying to detect the gravitational wave (GW) signal through the long-term observation of pulsars. Recently the NANOGrav reported the hint of the stochastic GW signal in their 12.5-year observation [1]. This signal can be explained by the stochastic GW with  $\Omega_{\text{GW}} \sim 10^{-9}$  at  $f \sim 10^{-8}\text{Hz}$ , which can be sourced by cosmic string [2–5], the phase transition [6–9] and the large density fluctuations in primordial black hole (PBH) formation models [10–15].

The PBH formation scenario is an attractive candidate for the NANOGrav signal since we can simultaneously explain the observed  $30M_{\odot}$  black holes in the binary merger events in LIGO-Virgo collaboration [16–19]. The PBH formation requires the large curvature power spectrum ( $\mathcal{P}_{\zeta}(k_{\text{pbh}}) \sim 0.02$ ) at a wavenumber  $k_{\text{pbh}}$  related to the mass of the formed PBHs. Since PBHs are formed when the high-density regions enter the horizon and collapse, the PBH mass is roughly given by the horizon mass at the collapse, which is related to the frequency of the density fluctuation  $f$  ( $= k_{\text{pbh}}/2\pi$ ) as [20]

$$M(f) \simeq 30M_{\odot} \left(\frac{\gamma}{0.2}\right) \left(\frac{g_*}{10.75}\right)^{-1/6} \left(\frac{f}{5.3 \times 10^{-10} \text{ Hz}}\right)^{-2}, \quad (1)$$

where  $\gamma \sim 0.2$  is a ratio of PBH mass to the horizon mass and  $g_*$  is the relativistic degree of freedom at the PBH formation. The same density fluctuations produce GWs through the nonlinear coupling,  $\langle \zeta \zeta h \rangle$  when they enter the horizon. Those induced GWs have  $f \sim 10^{-9}\text{Hz}$ , which is close to the frequency of the NANOGrav signal.

In this paper, we focus on the axion-like curvaton model of the PBH formation scenario [12, 21–24]. There are two types of the axion-like curvaton models; in one type the complex field  $\Phi$  (whose phase part is the axion) rolls down toward origin during inflation [12, 21–23], and in the other type  $\Phi$  rolls down from the origin [24]. These two types lead to the different dynamics and the power spectrum of induced GWs. The former type (type I) has been already studied and successfully explains the NANOGrav signal [12]. In this paper, we investigate whether the latter type (type II) can explain the NANOGrav signal. The type II model was first proposed in [24] where the model parameters are chosen to achieve the narrow density power spectrum of the density perturbations. However, a broader power spectrum is preferable to account for the NANOGrav signal. Thus, we investigate whether such a broad power spectrum can be produced in this paper. It is found that by choosing appropriate parameters of the potential term in Eq. (15), we obtain the broader spectral shape. We also improve the treatment of the non-Gaussianity of this model to estimate the amplitude of the induced GW precisely.

This paper is organized as follows. We calculate the curvature power spectrum of the type II axion-like curvaton model in Sec. 2. Next, we calculate the PBH abundance in Sec. 3 and induced GWs in Sec. 4. We can achieve the broad power spectrum of induced GWs and explain the NANOGrav signal. In Sec. 5, we conclude this paper.

## 2 Type II axion-like curvaton model

Let us briefly explain the type II axion-like curvaton model. (See [24] for the detailed calculation.) In this model, large fluctuations are produced in the phase direction of a complex scalar field  $\Phi$ , which we call ‘‘axion-like curvaton’’. The potential of  $\Phi$  is given by [24]

$$V_{\Phi} = \frac{\lambda}{4} \left( |\Phi|^2 - \frac{v^2}{2} \right)^2 + gI^2|\Phi|^2 - v^3\epsilon(\Phi + \Phi^*), \quad (2)$$

where  $I$  is the inflaton field,  $\lambda$  and  $g$  are coupling constants,  $v/\sqrt{2}$  is the vacuum expectation value after inflation. The bias term,  $v^3\epsilon(\Phi + \Phi^*)$ , is introduced to avoid the cosmic string problem, which is naturally small ( $\epsilon \ll 1$ ) in the sense of ‘t Hooft’s naturalness [25] since  $U(1)$  symmetry is restored for  $\epsilon = 0$ .

The field value of  $\Phi$  changes during inflation due to the first and second term of Eq. (2). In the early stage of inflation ( $I \gtrsim (\lambda/g)^{1/2}v$ ), the interaction term with the inflaton fixes  $\Phi$  near the origin. In the late stage, the inflaton field value becomes smaller and  $\Phi$  starts to roll down the Higgs-like potential towards  $|\Phi| = v$ . In this dynamics the phase direction acquires large fluctuations  $\sim H/|\Phi|$  ( $H$ : Hubble parameter during inflation).

The PBH formation requires the large fluctuations with wavenumber  $k = k_{\text{pbh}} \simeq 10^5 \text{ Mpc}^{-1}$ , which corresponds to the scale of  $30M_{\odot}$  PBHs. Thus, we determine the inflaton coupling  $g$  so that  $\Phi$  starts to roll down potential at  $t_{\text{pbh}}$  satisfying  $H(t_{\text{pbh}}) = k_{\text{pbh}}/a(t_{\text{pbh}})$ , which leads to

$$g \simeq \frac{\lambda}{4} \left( \frac{v}{I(t_{\text{pbh}})} \right)^2. \quad (3)$$

We also assume that the effective mass of  $\Phi$  is much larger than the Hubble parameter ( $\lambda v^2 \gg H^2$ ) until  $t_{\text{pbh}}$  to suppress the fluctuation at the larger wavelengths. This condition also ensures independence on the initial condition since  $\Phi$  settles near the origin of the potential independent of the initial field value of  $\Phi$ .

Based on the above background field dynamics, we calculate the fluctuation of  $\Phi$ , which is decomposed as

$$\Phi = \frac{1}{\sqrt{2}}(\varphi_0 + \varphi)e^{i\theta} \quad (4)$$

with the homogeneous solution  $\varphi_0$ , and the perturbations  $\varphi$  and  $\theta$ . The phase direction  $\theta$  works as the curvaton, and the canonical field of the phase direction is defined as  $\tilde{\sigma} \equiv \varphi_0\theta$ . The inflation induces the quantum fluctuations with amplitude  $H/(2\pi)$  for  $\tilde{\sigma}$  at the horizon crossing. Thus, the power spectrum of the  $\theta$  fluctuations is given by

$$\mathcal{P}_\theta(k, t_k) = \left( \frac{H(t_k)}{2\pi\varphi_0(t_k)} \right)^2, \quad (5)$$

where  $t_k$  is the time when the fluctuation with  $k$  crosses the horizon.  $\mathcal{P}_\theta(k, t_k)$  is suppressed for  $k > k_{\text{pbh}}$  since the  $\varphi_0(t_k)$  quickly grows after  $t_{\text{pbh}}$ . While the  $\Phi$  is fixed near the origin before  $t_{\text{pbh}}$ ,  $\tilde{\sigma}$  has the large effective mass given by

$$\tilde{m}_\sigma^2 \equiv \left. \frac{\partial^2 (-v^3\epsilon(\Phi + \Phi^*))}{\partial\tilde{\sigma}^2} \right|_{\tilde{\sigma}=0} = \sqrt{2}\epsilon v^2 \frac{v}{\varphi_0}. \quad (6)$$

where we choose the model parameter so as  $m_\sigma^2 > H^2$  for  $t < t_{\text{pbh}}$ . Such large effective mass damps the fluctuations as  $\tilde{\sigma} \propto a^{-3/2}$ , and we define the damping factor of the phase direction with momentum  $k$  as

$$R_k \equiv \left( \frac{\tilde{\sigma}_k(t_{\text{pbh}})}{\tilde{\sigma}_k(t_k)} \right) \sim \left( \frac{k}{k_{\text{pbh}}} \right)^{3/2} \quad \text{for } k < k_{\text{pbh}}. \quad (7)$$

( $R_k = 1$  for  $k > k_{\text{pbh}}$ .) Finally, the power spectrum of the  $\theta$  fluctuations at the end of inflation  $t_e$  is given by

$$P_\theta(k, t_e) = R_k^2 \mathcal{P}_\theta(k, t_k). \quad (8)$$

Let us evaluate the density perturbations induced by the fluctuations of the phase direction. We suppose that the curvaton obtains the axion-like potential after inflation through some nonperturbative effect. The potential minimum of the nonperturbative term does not coincide with that of the primordial one determined by the bias term in our model. Suppose that nonperturbative potential takes the minimum at  $\theta = \theta_i$ , then it is written as

$$V_\sigma = \Lambda^4 [1 - \cos(\Theta)] \simeq \frac{1}{2} m_\sigma^2 \sigma^2, \quad (9)$$

where  $\Theta \equiv \theta - \theta_i$ , the curvaton  $\sigma$  is defined as  $\sigma \equiv v\Theta$  and  $m_\sigma = \Lambda^2/v$ . We assume that  $m_\sigma$  is small enough to neglect the axion-like potential during inflation, i.e.  $H^2 \gg m_\sigma^2$ . The density fluctuation is given by  $\delta\rho_\sigma/\rho_\sigma = 2\delta\theta/\theta_i$ .

The power spectrum of curvature perturbations is given by

$$\mathcal{P}_\zeta(k) = \left( \frac{r}{4+3r} \right)^2 \left( \frac{2}{\theta_i} \right)^2 \mathcal{P}_\theta(k, t_k) R_k^2. \quad (10)$$

where  $r$  is the ratio of the energy density of the curvaton to that of the inflaton (or radiation after reheating),  $r = \rho_\sigma/\rho_I$ . Assuming the instant reheating at  $t_{\text{reheat}}$ , the ratio is given by  $r(t_{\text{reheat}}) = (v^2\theta_i^2)/(6M_{pl}^2)$ , which is chosen to be small to ensure that  $\Phi$  does not disturb the inflation.  $r$  grows during radiation-dominated era as  $r \propto a$  due to the matter-like behavior of the curvaton, and its growth ends at the curvaton decay,  $t_{\text{decay}}$ . We require that the curvaton decays into radiation before it overcloses the universe,  $r(t_{\text{decay}}) \sim 0.5$ , at which the temperature of the universe is  $T_{\text{decay}} \sim (r(t_{\text{reheat}})/r(t_{\text{decay}}))T_{\text{reheat}}$ . The typical decay rate of  $\Phi$  is related to the curvaton mass as  $\Gamma_\sigma = \kappa^2 m_\sigma^3/(16\pi v^2)$  where  $\kappa$  is a coupling constant. We confirm that  $T_{\text{decay}} \sim 10^3 \text{GeV}$  is achieved for  $m_\sigma \sim 10^8 \text{GeV}$  for our parameters in Eq. (15). In the following,  $r$  refers to the energy ratio after decay, that is  $r \equiv r(t_{\text{decay}})$ .

The PBH abundance highly depends on non-Gaussian distribution of  $\mathcal{P}_\zeta(k)$ . It is known that the axion-like curvaton models produce large non-Gaussianity with local type bispectrum characterized by the following parameter: [23]

$$f_{\text{NL}} = \frac{5}{12} \left( -3 + \frac{4}{r} + \frac{8}{4+3r} \right). \quad (11)$$

We discuss the enhancement of the PBH abundance by non-Gaussianity in Sec.3. Non-Gaussianity also affects the power spectrum of the curvature perturbations and induced gravitational wave through the higher-order correlations [26,27], whose contribution is characterized by  $\mathcal{P}_\zeta f_{\text{NL}}^2$ . We take the non-Gaussianity into account approximately since non-Gaussian is small compared to the Gaussian contribution in our parameter set given by Eq. (15),  $\mathcal{P}_\zeta f_{\text{NL}}^2 < 0.04$ . We estimate non-Gaussian amplification on the curvature power spectrum as

$$\begin{aligned} Q_{\mathcal{P}}^{(\text{NL})} &\equiv \frac{\mathcal{P}_\zeta^{(\text{NL})}(k_*)}{\mathcal{P}_\zeta(k_*)} \\ &= 1 + \left( \frac{3}{5} f_{\text{NL}} \right)^2 \frac{k_*^3}{2\pi \mathcal{P}_\zeta(\mathbf{k}_*)} \int d^3q \frac{\mathcal{P}_\zeta(\mathbf{q}) \mathcal{P}(|\mathbf{k}_* - \mathbf{q}|)}{q^3 |\mathbf{k}_* - \mathbf{q}|^3}, \end{aligned} \quad (12)$$

where  $k_*$  is the wavenumber at the peak of  $\mathcal{P}_\zeta$ .  $Q_{\mathcal{P}}^{(\text{NL})}$  is about 1.07 for  $r = 0.5$  and 1.01 for  $r = 1.0$  in our parameter set.

Finally, the power spectrum of the density perturbations is given by

$$\mathcal{P}_\delta(k, t) = \left( \frac{2}{3} \frac{k}{a(t)H(t)} \right)^4 T(k\eta(t))^2 \mathcal{P}_\zeta(k), \quad (13)$$

where  $\eta(t)$  is the conformal time and  $T(x)$  is the transfer function during radiation dominated era, which includes the suppression of the density perturbation in sub-horizon as

$$T(x) \equiv 3 \frac{\sin(x/\sqrt{3}) - (x/\sqrt{3}) \cos(x/\sqrt{3})}{(x/\sqrt{3})^3}. \quad (14)$$

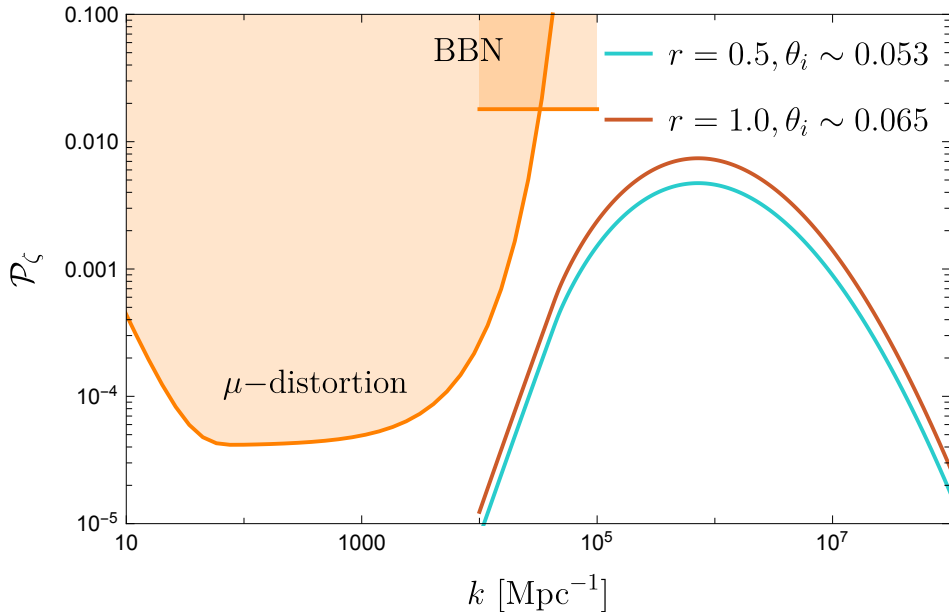


Figure 1: The curvature power spectrum  $Q_{\mathcal{P}}^{(\text{NL})}\mathcal{P}_{\zeta}(k)$  based on Eqs.(10) and (12). The non-Gaussian contribution is included by  $Q_{\mathcal{P}}^{(\text{NL})}$ . The orange regions are constraints on the curvature power spectrum from  $\mu$ -distortion [28] by COBE/FIRAS [29] and BBN [30].

In this paper, we use the following set of model parameters:

$$\begin{aligned}
 \lambda &= 7.5 \times 10^{-6}, & v &= 5.77 \times 10^{-2} M_{\text{pl}}, \\
 g &= 9.56 \times 10^{-11}, & \epsilon &= 2.57 \times 10^{-10}, \\
 \left\{ \begin{array}{l} r = 0.5, \quad \theta_i = 5.3 \times 10^{-2} \\ r = 1.0, \quad \theta_i = 6.5 \times 10^{-2} \end{array} \right. & & & (15)
 \end{aligned}$$

where we take  $r$  and  $\theta_i$  to achieve the PBH abundance required to explain the LIGO-Virgo event rate. Compared to the previous paper [24], we use smaller  $v$ ,  $g$  and  $\lambda$  to achieve a broad power spectrum. We numerically evaluate the dynamics of  $\Phi$  assuming the chaotic inflation whose potential is given by  $V_I = m_I^2 I^2/2$  with  $m_\phi \simeq 10^{13} \text{GeV}$ . The similar dynamics also holds for other inflation models. We show the curvature power spectrum  $\mathcal{P}_{\zeta}(k)$  [Eq. (10)] in Fig. 1. Although we use the broad power spectrum, they avoid the constraints on  $\mu$ -distortion [28] by COBE/FIRAS [29] and BBN [30].

### 3 PBH formation

The PBHs are formed by the collapse of high-density regions when they re-enter the horizon. The criterion on the PBH formation is estimated by the numerical simulation [31], in which

the threshold value of the averaged density fluctuation is obtained. Since the threshold value is too large to neglect the nonlinear contribution, we need to use the effective threshold value including the nonlinear relation between density and curvature perturbations. The detailed analysis show that the effective threshold value is  $\delta_{\text{th(eff)}} \simeq \sqrt{2} \times 0.53$  for the averaged linear density perturbation defined by [32]

$$\begin{aligned}\bar{\delta}_R(\mathbf{x}) &\equiv \int d^3y W(|\mathbf{x} - \mathbf{y}|, R) \delta(\mathbf{y}) \\ &= \int \frac{d^3p}{(2\pi)^3} \tilde{W}(pR) e^{i\mathbf{p}\cdot\mathbf{x}} \delta_p,\end{aligned}\tag{16}$$

where  $R = k^{-1}$  is the scale of the horizon corresponding to the PBH mass [Eq.(1)],  $W(x, R)$  and  $\tilde{W}(z)$  are the window functions in the real and Fourier spaces, and the  $\delta_p$  is the density fluctuation. Although it is known that the choice of window function causes a large uncertainty [33], the natural choice is the real-space top-hat window function used in the threshold value in the numerical simulation,

$$\tilde{W}(z) = 3 \frac{\sin(z) - z \cos(z)}{z^3}.\tag{17}$$

Thus, a PBH is formed when a region has the averaged density  $\bar{\delta}_R$  larger than the threshold value  $\delta_{\text{th(eff)}}$ .

We estimate the PBH formation rate based on the Press–Schechter formalism, where the PBH formation rate is calculated by the probability distribution of the averaged density perturbations. In our model,  $\bar{\delta}_R$  follows the non-Gaussian distribution due to  $f_{\text{NL}}$  given by Eq. (11), which drastically changes the PBH abundance. The probability distribution of  $\bar{\delta}_R$  is characterized by the variance and skewness defined by

$$\sigma_R^2 = \langle \bar{\delta}_R^2 \rangle - \langle \bar{\delta}_R \rangle^2,\tag{18}$$

$$\mu_R = \sigma_R^{-3} \left( \langle \bar{\delta}_R^3 \rangle - 3 \langle \bar{\delta}_R^2 \rangle \langle \bar{\delta}_R \rangle + 2 \langle \bar{\delta}_R \rangle^3 \right).\tag{19}$$

where  $\langle \dots \rangle$  describes the ensemble average of  $\delta_p$ . For simplicity, we neglect the scale dependence of  $\mu_R$  and evaluate it at  $R = R_{\text{pbh}} = k_{\text{pbh}}^{-1}$ , which corresponds to  $30M_{\odot}$  PBHs. Using the formula in [32], the skewness is numerically given by

$$\mu \equiv \mu_R|_{R=R_{\text{pbh}}} \simeq 3.39 f_{\text{NL}} \sigma_R|_{R=R_{\text{pbh}}}.\tag{20}$$

We construct the statistical variable which reproduces the probability distribution of  $\bar{\delta}_R$ . Using the Gaussian variable  $\chi$  characterized by  $\langle \chi^2 \rangle = \sigma_R^2$ , we define the statistical variable as

$$\bar{\delta}[\chi] \equiv \chi + \frac{\mu}{6\sigma_R} (\chi^2 - \sigma_R^2),\tag{21}$$

which has the same variance and skewness in Eqs. (18) and (19) up to  $\mathcal{O}(f_{\text{NL}}\sigma_R)$ . The probability distribution of  $\bar{\delta}[\chi]$  is given by [34–36]

$$P_R^{(\text{NG})}(\bar{\delta}) = \sum_{i=\pm} \left| \frac{d\chi_i(\bar{\delta})}{d\bar{\delta}} \right| P_R^{(\text{G})}(\chi_i(\bar{\delta})), \quad (22)$$

where  $P_R^{(\text{G})}(\chi)$  is the Gaussian distribution function,

$$P_R^{(\text{G})}(\chi) = \frac{1}{\sqrt{2\pi}\sigma_R} \exp\left(-\frac{1}{2}\frac{\chi^2}{\sigma_R^2}\right), \quad (23)$$

and  $\chi_{\pm}(\bar{\delta})$  are two solutions of  $\bar{\delta} = \bar{\delta}[\chi]$ ,

$$\chi_{\pm}(\bar{\delta}) = \frac{3\sigma_R}{\mu} \left( -1 \pm \sqrt{1 + \frac{2\mu}{3} \left( \frac{\mu}{6} + \frac{\bar{\delta}}{\sigma_R} \right)} \right). \quad (24)$$

The PBH formation rate is given by the probability of  $\bar{\delta} > \delta_{\text{th(eff)}}$ , which leads to

$$\begin{aligned} \beta(R) &= \int_{\bar{\delta} > \delta_{\text{th(eff)}}} P_R^{(\text{NG})}(\bar{\delta}) d\bar{\delta} = \int_{\bar{\delta}[\chi] > \delta_{\text{th(eff)}}} P_R^{(\text{G})}(\chi) d\chi \\ &\simeq \frac{\sigma_R}{\sqrt{2\pi}\chi_+(\delta_{\text{th(eff)})}} \exp\left(-\frac{\chi_+(\delta_{\text{th(eff)})}^2}{2\sigma_R^2}\right). \end{aligned} \quad (25)$$

Here we have used  $\mu > 0$  and  $\chi_+(\delta_{\text{th(eff)})}/\sigma_R \gg 1$  in the last line. The present PBH abundance is given by

$$f(M) \equiv \frac{d\Omega_{\text{PBH}}}{d \ln M} \frac{1}{\Omega_{\text{DM}}} \quad (26)$$

$$= \frac{\beta(R(M))}{1.8 \times 10^{-8}} \left( \frac{\gamma}{0.2} \right)^{3/2} \left( \frac{10.75}{g_*} \right)^{1/4} \left( \frac{0.12}{\Omega_{\text{DM}} h^2} \right) \left( \frac{M}{M_{\odot}} \right)^{-1/2}, \quad (27)$$

where  $g_*$  is the relativistic degree of freedom at  $T \sim 30\text{MeV}$ .

We show the calculated mass spectrum of PBH in Fig. 2. We also plot the relevant constrains by microlensing experiments ‘‘MACHO/EROS/OGLE’’ [37–39] and energy injection into CMB through accretion around PBHs [40]. Since our model predicts the broad mass distribution, the large mass part of the distribution could conflict with the accretion constraints. However, it is noticed that accretion constraint has a large uncertainty. In fact, two different constraints are obtained depending on assumptions as shown in Fig. 2. Our mass distribution is consistent if we adopt the weaker accretion constraint.

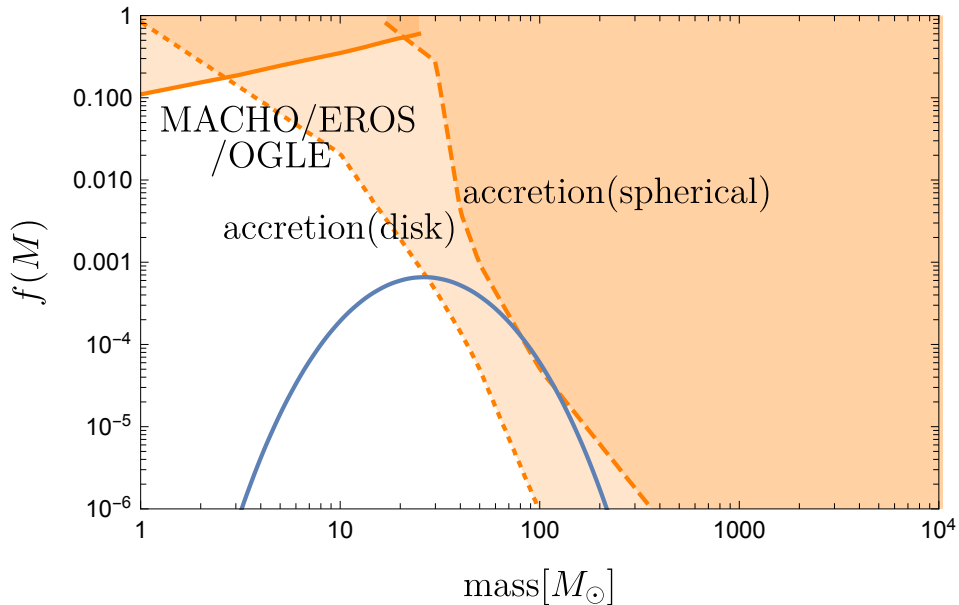


Figure 2: The mass spectrum of PBHs (blue line) and the constraints (orange regions) by microlensing experiments “MACHO/EROS/OGLE” (solid line) [37–39], CMB through spherical accretion (dashed line) and disk accretion (dotted line) [40].

## 4 Induced gravitational wave

The large density fluctuations induce the gravitational waves through the nonlinear coupling  $\langle \zeta \zeta h \rangle$  when they re-enter the horizon. The current energy fraction of GWs is written as

$$\begin{aligned} \Omega_{\text{GW}}(t_0, k) &= \left( \frac{a_c^2 H_c}{a_0^2 H_0} \right)^2 \Omega_{\text{GW}}(\eta_c, k) \\ &\simeq 0.83 \left( \frac{g_c}{10.75} \right)^{-1/3} \Omega_{r,0} \Omega_{\text{GW}}(t_c, k), \end{aligned} \quad (28)$$

where  $\Omega_{r,0}$  is the current energy fraction of radiation, the subscript “c” denotes values when GW production effectively finishes.

The energy density of the induced GWs at  $t_c$  is calculated by solving the equation of motion of GWs with the source term of scalar fluctuations, and it is given by [20]

$$\begin{aligned} \Omega_{\text{GW}}(t_c, k) &= \frac{8}{243} \int_0^\infty dy \int_{|1-y|}^{1+y} dx \mathcal{P}_\zeta(kx) \mathcal{P}_\zeta(ky) \frac{y^2}{x^2} \\ &\times \left( 1 - \frac{(1+y^2-x^2)^2}{4y^2} \right)^2 \overline{\mathcal{I}(x, y, \eta_c)^2}, \end{aligned} \quad (29)$$

where overline means the time average over  $\eta_c$ .  $\mathcal{I}(x, y, \eta_c)$  is written as

$$\mathcal{I}(x, y, \eta_c) = \frac{k^2}{a(\eta_c)} \int^{\eta_c} d\bar{\eta} a(\bar{\eta}) g_k(\eta_c; \bar{\eta}) f(ky, kx, \bar{\eta}). \quad (30)$$

Here  $g_k$  is the Green function,

$$g_k(\eta, \tilde{\eta}) = \frac{\sin(k(\eta - \tilde{\eta}))}{k} \theta(\eta - \tilde{\eta}), \quad (31)$$

and  $f(k_1, k_2, \eta)$  is given by

$$f(k_1, k_2, \eta) = \left[ 2T(k_1, \eta)T(k_2, \eta) + \left( \frac{\dot{T}(k_1, \eta)}{H(\eta)} + T(k_1, \eta) \right) \left( \frac{\dot{T}(k_2, \eta)}{H(\eta)} + T(k_2, \eta) \right) \right], \quad (32)$$

where  $T(x)$  is the transfer function of the scalar fluctuations given by Eq.(14).

We comment on the non-Gaussian contribution on the induced gravitational waves [26, 27]. It is pointed out in [27] that non-Gaussianity of scalar fluctuations amplifies the induced gravitational waves when  $\mathcal{P}_\zeta f_{\text{NL}}^2$  is large. Since  $\mathcal{P}_\zeta f_{\text{NL}}^2 < 0.04$  in our calculation, the effect of non-Gaussianity is expected to be sub-dominant. Thus, we approximately include the effect of the non-Gaussianity on  $\Omega_{\text{GW}}$  by multiplying the factor  $(Q_{\mathcal{P}}^{\text{NL}})^2$  given by Eq. (12). This approximation includes a part of non-Gaussian contributions, ‘‘Hybrid’’ and ‘‘Reducible’’-type terms discussed in [26]. Hybrid type is a product of the Gaussian and non-Gaussian contribution of curvature perturbation, and Reducible type is that of non-Gaussian and non-Gaussian contribution. Although there are other types of sources of GWs, it is known that Hybrid-type is one of the largest contributions among them. Thus, our calculation can estimate most of the effects of non-Gaussianity.

The estimated GW spectra for  $r = 0.5$  (blue line) and  $r = 1.0$  (orange line) are shown in Fig. 3. The GW spectrum observed by the NANOGrav experiment is fitted by the power-law spectrum around  $f \sim 10^{-8}$ ,

$$\Omega_{\text{GW}}(f)h^2 = \frac{2\pi^2}{3} \frac{h^2 f^2}{H_0^2} h_c^2(f) = A_\Omega f^{5-\gamma}, \quad (33)$$

where  $\gamma$  is a tilt of the spectrum. In Fig. 3, we show the observed GWs for  $\gamma = 5$  and 6 with  $2\text{-}\sigma$  uncertainty on  $A_\Omega$ . We also plot current constraints by other PTA experiments, EPTA (solid) [41] and PPTA (dotted) [42], and future sensitivity by SKA (dashed) [43]. It is found that the broad power spectrum of GWs in the present model can explain the reported NANOGrav signal.

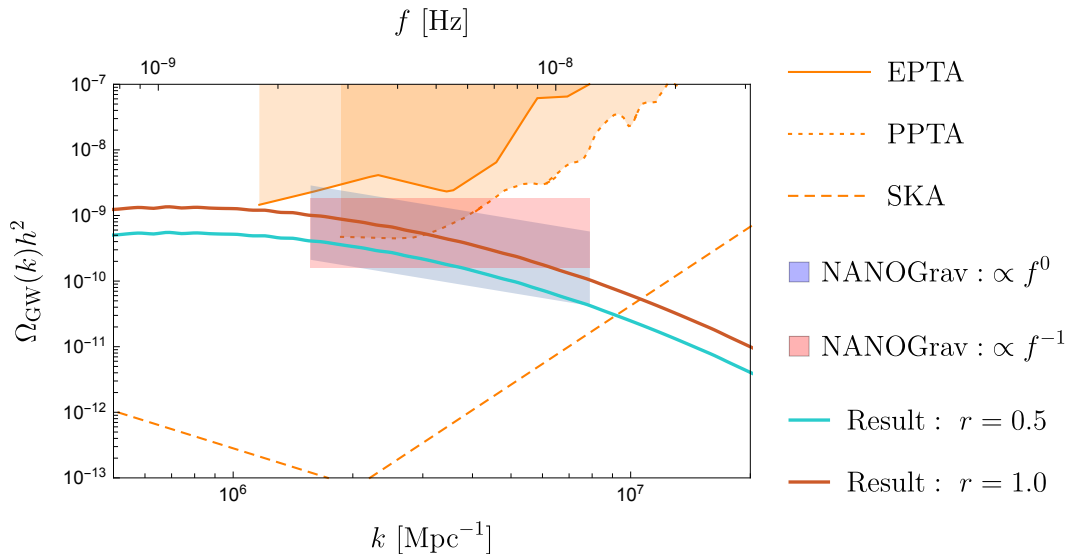


Figure 3: The induced GW spectrum and the constraints by PTA experiments. We include the contribution of non-Gaussianity by using the factor  $Q_{\mathcal{P}}^{(\text{NL})}$ . The orange lines are current constraints by EPTA (solid) [41] and PPTA (Dotted) [42], and future sensitivity by SKA (Dashed) [43]. We show the reported NANOGrav signal with  $\gamma = 5$  (blue region) and  $\gamma = 6$  (pink region) with  $2\text{-}\sigma$  uncertainty (see Eq. (33)).

## 5 Conclusion

The reported signal by the NANOGrav experiment indicates the various cosmological phenomena like cosmic string, phase transition and PBH formation. The PBH formation scenario is attractive among them since the reported frequency  $f \sim 10^{-8}\text{Hz}$  is close to the scale of the density fluctuations to produce  $30M_{\odot}$  PBH, which can explain the binary black holes observed by LIGO-Virgo collaboration.

The typical PBH formation models predict the induced GWs with smaller frequency and larger amplitude compared to the NANOGrav signal. To avoid this difficulty, one needs to modify the induced GW spectrum by the broad power spectrum and the non-Gaussianity of density fluctuations, which can enhance the PBH formation rate and give a good fit to the NANOGrav signal. The axion-like curvaton model can achieve the required features.

There are two types of the axion-like curvaton models; in type I the complex field rolls down toward origin during inflation [12, 21–23], and in type II it rolls down from the origin [24]. In this paper, we focused on the type II model and chose the appropriate parameters of the potential term, which leads to a broader power spectrum of the density perturbations than that in [24]. As a result it was found that the induced GW spectrum can explain the NANOGrav signal as

shown in Fig. 3. Moreover, the broad power spectrum of the density fluctuation results in the broad mass spectrum of PBHs as shown in Fig. 2, which can be tested by the accumulation of the binary merger observations.

## References

- [1] NANOGrav collaboration, Z. Arzoumanian et al., *The NANOGrav 12.5-year Data Set: Search For An Isotropic Stochastic Gravitational-Wave Background*, [2009.04496](#).
- [2] J. Ellis and M. Lewicki, *Cosmic String Interpretation of NANOGrav Pulsar Timing Data*, [2009.06555](#).
- [3] S. Blasi, V. Brdar and K. Schmitz, *Has NANOGrav found first evidence for cosmic strings?*, [2009.06607](#).
- [4] W. Buchmuller, V. Domcke and K. Schmitz, *From NANOGrav to LIGO with metastable cosmic strings*, *Phys. Lett. B* **811** (2020) 135914, [[2009.10649](#)].
- [5] R. Samanta and S. Datta, *Gravitational wave complementarity and impact of NANOGrav data on gravitational leptogenesis: cosmic strings*, [2009.13452](#).
- [6] Y. Nakai, M. Suzuki, F. Takahashi and M. Yamada, *Gravitational Waves and Dark Radiation from Dark Phase Transition: Connecting NANOGrav Pulsar Timing Data and Hubble Tension*, [2009.09754](#).
- [7] A. Addazi, Y.-F. Cai, Q. Gan, A. Marciano and K. Zeng, *NANOGrav results and Dark First Order Phase Transitions*, [2009.10327](#).
- [8] A. Neronov, A. Roper Pol, C. Caprini and D. Semikoz, *NANOGrav signal from MHD turbulence at QCD phase transition in the early universe*, [2009.14174](#).
- [9] S.-L. Li, L. Shao, P. Wu and H. Yu, *NANOGrav Signal from First-Order Confinement/Deconfinement Phase Transition in Different QCD Matters*, [2101.08012](#).
- [10] V. Vaskonen and H. Veermäe, *Did NANOGrav see a signal from primordial black hole formation?*, [2009.07832](#).
- [11] V. De Luca, G. Franciolini and A. Riotto, *NANOGrav Hints to Primordial Black Holes as Dark Matter*, [2009.08268](#).
- [12] K. Inomata, M. Kawasaki, K. Mukaida and T. T. Yanagida, *NANOGrav results and LIGO-Virgo primordial black holes in axion-like curvaton model*, [2011.01270](#).
- [13] K. Kohri and T. Terada, *Solar-Mass Primordial Black Holes Explain NANOGrav Hint of Gravitational Waves*, *Phys. Lett. B* **813** (2021) 136040, [[2009.11853](#)].

- [14] G. Domènech and S. Pi, *NANOGrav Hints on Planet-Mass Primordial Black Holes*, [2010.03976](#).
- [15] S. Sugiyama, V. Takhistov, E. Vitagliano, A. Kusenko, M. Sasaki and M. Takada, *Testing Stochastic Gravitational Wave Signals from Primordial Black Holes with Optical Telescopes*, [2010.02189](#).
- [16] LIGO SCIENTIFIC, VIRGO collaboration, B. P. Abbott et al., *Binary Black Hole Population Properties Inferred from the First and Second Observing Runs of Advanced LIGO and Advanced Virgo*, [1811.12940](#).
- [17] S. Bird, I. Cholis, J. B. Muñoz, Y. Ali-Haïmoud, M. Kamionkowski, E. D. Kovetz et al., *Did LIGO detect dark matter?*, *Phys. Rev. Lett.* **116** (2016) 201301, [[1603.00464](#)].
- [18] S. Clesse and J. García-Bellido, *The clustering of massive Primordial Black Holes as Dark Matter: measuring their mass distribution with Advanced LIGO*, *Phys. Dark Univ.* **15** (2017) 142–147, [[1603.05234](#)].
- [19] M. Sasaki, T. Suyama, T. Tanaka and S. Yokoyama, *Primordial Black Hole Scenario for the Gravitational-Wave Event GW150914*, *Phys. Rev. Lett.* **117** (2016) 061101, [[1603.08338](#)].
- [20] K. Inomata, M. Kawasaki, K. Mukaida and T. T. Yanagida, *Double inflation as a single origin of primordial black holes for all dark matter and LIGO observations*, *Phys. Rev. D* **97** (2018) 043514, [[1711.06129](#)].
- [21] M. Kawasaki, N. Kitajima and T. T. Yanagida, *Primordial black hole formation from an axionlike curvaton model*, *Phys. Rev. D* **87** (2013) 063519, [[1207.2550](#)].
- [22] M. Kawasaki, N. Kitajima and S. Yokoyama, *Gravitational waves from a curvaton model with blue spectrum*, *JCAP* **1308** (2013) 042, [[1305.4464](#)].
- [23] K. Ando, K. Inomata, M. Kawasaki, K. Mukaida and T. T. Yanagida, *Primordial Black Holes for the LIGO Events in the Axion-like Curvaton Model*, [1711.08956](#).
- [24] K. Ando, M. Kawasaki and H. Nakatsuka, *Formation of primordial black holes in an axionlike curvaton model*, *Phys. Rev. D* **98** (2018) 083508, [[1805.07757](#)].
- [25] G. 't Hooft, *Naturalness, chiral symmetry, and spontaneous chiral symmetry breaking*, *NATO Sci. Ser. B* **59** (1980) 135–157.
- [26] C. Unal, *Imprints of Primordial Non-Gaussianity on Gravitational Wave Spectrum*, *Phys. Rev. D* **99** (2019) 041301, [[1811.09151](#)].
- [27] R.-g. Cai, S. Pi and M. Sasaki, *Gravitational Waves Induced by non-Gaussian Scalar Perturbations*, *Phys. Rev. Lett.* **122** (2019) 201101, [[1810.11000](#)].

- [28] J. Chluba, A. L. Erickcek and I. Ben-Dayan, *Probing the inflaton: Small-scale power spectrum constraints from measurements of the cosmic microwave background energy spectrum*, *The Astrophysical Journal* **758** (2012) 76.
- [29] D. J. Fixsen, E. S. Cheng, J. M. Gales, J. C. Mather, R. A. Shafer and E. L. Wright, *The Cosmic Microwave Background spectrum from the full COBE FIRAS data set*, *Astrophys. J.* **473** (1996) 576, [[astro-ph/9605054](#)].
- [30] K. Inomata, M. Kawasaki and Y. Tada, *Revisiting constraints on small scale perturbations from big-bang nucleosynthesis*, *Phys. Rev.* **D94** (2016) 043527, [[1605.04646](#)].
- [31] M. Shibata and M. Sasaki, *Black hole formation in the Friedmann universe: Formulation and computation in numerical relativity*, *Phys. Rev. D* **60** (1999) 084002, [[gr-qc/9905064](#)].
- [32] M. Kawasaki and H. Nakatsuka, *Effect of nonlinearity between density and curvature perturbations on the primordial black hole formation*, *Phys. Rev. D* **99** (2019) 123501, [[1903.02994](#)].
- [33] K. Ando, K. Inomata and M. Kawasaki, *Primordial black holes and uncertainties on choice of window function*, [1802.06393](#).
- [34] S. Young and C. T. Byrnes, *Primordial black holes in non-Gaussian regimes*, *JCAP* **1308** (2013) 052, [[1307.4995](#)].
- [35] C. T. Byrnes, E. J. Copeland and A. M. Green, *Primordial black holes as a tool for constraining non-Gaussianity*, *Phys. Rev.* **D86** (2012) 043512, [[1206.4188](#)].
- [36] S. Young, D. Regan and C. T. Byrnes, *Influence of large local and non-local bispectra on primordial black hole abundance*, *JCAP* **1602** (2016) 029, [[1512.07224](#)].
- [37] MACHO collaboration, R. A. Allsman et al., *MACHO project limits on black hole dark matter in the 1-30 solar mass range*, *Astrophys. J.* **550** (2001) L169, [[astro-ph/0011506](#)].
- [38] EROS-2 collaboration, P. Tisserand et al., *Limits on the Macho Content of the Galactic Halo from the EROS-2 Survey of the Magellanic Clouds*, *Astron. Astrophys.* **469** (2007) 387–404, [[astro-ph/0607207](#)].
- [39] L. Wyrzykowski et al., *The OGLE View of Microlensing towards the Magellanic Clouds. IV. OGLE-III SMC Data and Final Conclusions on MACHOs*, *Mon. Not. Roy. Astron. Soc.* **416** (2011) 2949, [[1106.2925](#)].

- [40] P. D. Serpico, V. Poulin, D. Inman and K. Kohri, *Cosmic microwave background bounds on primordial black holes including dark matter halo accretion*, *Phys. Rev. Res.* **2** (2020) 023204, [[2002.10771](#)].
- [41] L. Lentati et al., *European Pulsar Timing Array Limits On An Isotropic Stochastic Gravitational-Wave Background*, *Mon. Not. Roy. Astron. Soc.* **453** (2015) 2576–2598, [[1504.03692](#)].
- [42] R. M. Shannon et al., *Gravitational waves from binary supermassive black holes missing in pulsar observations*, *Science* **349** (2015) 1522–1525, [[1509.07320](#)].
- [43] C. J. Moore, R. H. Cole and C. P. L. Berry, *Gravitational-wave sensitivity curves*, *Class. Quant. Grav.* **32** (2015) 015014, [[1408.0740](#)].